

Compact Object Candidates with K/M-dwarf Companions from LAMOST Low-resolution Survey

Hui-Jun Mu¹, Wei-Min Gu^{2*}, Tuan Yi^{2*}, Ling-Lin Zheng², Hao Sou³, Zhong-Rui Bai^{4*}, Hao-Tong Zhang⁴,
Ya-Juan Lei⁴, and Cheng-Ming Li¹

¹International Laboratory for Quantum Functional Materials of Henan, and School of Physics and Microelectronics,
Zhengzhou University, Zhengzhou, Henan 450001, China;

²Department of Astronomy, Xiamen University, Xiamen, Fujian 361005, China;

³CAS Key Laboratory for Research in Galaxies and Cosmology, Department of Astronomy, University of Science
and Technology of China, Hefei, Anhui 230026, China;

⁴National Astronomical Observatories, Chinese Academy of Sciences, Beijing 100012, China

Received September 6, 2021; accepted November 5, 2021; published online December 29, 2021

Searching for compact objects (black holes, neutron stars, or white dwarfs) in the Milky Way is essential for understanding the stellar evolution history, the physics of compact objects, and the structure of our Galaxy. Compact objects in binaries with a luminous stellar companion are perfect targets for optical observations. Candidate compact objects can be achieved by monitoring the radial velocities of the companion star. However, most of the spectroscopic telescopes usually obtain stellar spectra at a relatively low efficiency, which makes a sky survey for millions of stars practically impossible. The efficiency of a large-scale spectroscopic survey, the Large Sky Area Multi-Object Fiber Spectroscopy Telescope (LAMOST), presents a specific opportunity to search for compact object candidates, i.e., simply from the spectroscopic observations. Late-type K/M stars are the most abundant populations in our Galaxy. Owing to the relatively large Keplerian velocities in the close binaries with a K/M-dwarf companion, a hidden compact object could be discovered and followed-up more easily. In this study, compact object candidates with K/M-dwarf companions are investigated with the LAMOST low-resolution stellar spectra. Based on the LAMOST Data Release 5, we obtained a sample of 56 binaries, each containing a K/M-dwarf with a large radial velocity variation $\Delta V_R > 150 \text{ km s}^{-1}$. Complemented with the photometric information from the Transiting Exoplanet Survey Satellite, we derived a sample of 35 compact object candidates, among which, the orbital periods of 16 sources were revealed by the light curves. Considering two sources as examples, we confirmed that a compact object existed in the two systems by fitting the radial velocity curve. This study demonstrates the principle and the power of searching for compact objects through LAMOST.

Spectroscopic binaries, Binary stars, Close binaries, Radial velocities, Stellar dynamics and kinematics

PACS number(s): 97.80.Fk, 97.80.-d, 97.80.Fk, 98.62.Py, 98.10.+z

Citation: H.-J. Mu, W.-M. Gu, T. Yi, L.-L. Zheng, H. Sou, Z.-R. Bai, H.-T. Zhang, Y.-J. Lei, and C.-M. Li., Compact Object Candidates with K/M-dwarf Companions from LAMOST Low-resolution Survey, *Sci. China-Phys. Mech. Astron.* **65**, 229711 (2022), <https://doi.org/10.1007/s11433-021-1809-8>

1 Introduction

Searching for compact objects (black holes (BH), neutron stars (NS), or white dwarfs (WD)) in the Milky Way is essential for understanding the stellar evolution history, the physics of compact objects, and the structure of our Galaxy. Compact objects are remnant products at the endpoint of stellar evolution. For progenitors at different stellar mass ranges, the type of compact object differs (WD: less than 8 solar mass (M_{\odot}); NS: 8-25 M_{\odot} ; BH: greater than 25 M_{\odot}). Most compact binaries have been discovered via signatures of accretion [1-9]. X-rays in X-ray binaries (XRBs) are produced by materials accreted from a secondary companion star onto a primary star. Recently, searching for compact objects in binary systems by utilizing large spectroscopic/photometric surveys has become a well-known strategy. The advantage of using optical database instead of conventional X-ray surveys is that it enables one to discover quiescent (noninteracting) systems. For example, by monitoring the radial velocities from large spectroscopic surveys, Thompson et al. [10] discovered 2MASS J05215658+4359220, which may contain a noninteracting low-mass BH ($3.3^{+2.8}_{-0.7}M_{\odot}$) or an unexpectedly high-mass NS; Liu et al. [11] reported LB-1, a wide binary which may contain an unusually massive BH ($68^{+11}_{-13}M_{\odot}$). Using a custom Monte Carlo sampler to analyze sparse, noisy, and poorly sampled radial velocities, Price-Whelan et al. [12] found faint companions in binary systems at different masses: high masses (BH candidates), low masses (substellar candidates), and very close separations (mass-transfer candidates). They identified 40 candidate noninteracting compact-object companions. By exploiting multiyear all-sky photometry from All-Sky Automated Survey for Supernovae, Rowan et al. [13] identified 369 candidates for ellipsoidal variability. By analyzing photometric light curves, WD+main sequence (MS) binaries showing eclipsing signals, such as those presented by Pyrzas et al. [14] can be detected. Although there are catalogs of compact objects and candidates (i.e., refs. [15-20]), more candidates are demanded by the astronomers to reveal the population. Owing to the large-scale spectroscopic survey of the Large Sky Area Multi-Object Fiber Spectroscopic Telescope (LAMOST [21-23]), an amazing opportunity for the search for compact objects has been presented.

In this study, we are going to focus on exploiting the spectroscopic surveys of LAMOST, which is located at the Xinglong Observatory, northeast of Beijing, China. It is characterized by both a large field of view (5 degrees field) and large effective aperture (3.6-4.9 meters). A total of 4000 fibers mounted on the focal plane make LAMOST facility a powerful tool with a high spectral acquisition rate [24]. The wavelength coverage is 3650-9000 Å. Around nine million low-resolution (with a spectral resolution $R \sim 1800$) spectra have been released through the Data Release (DR) 5 of LAMOST ¹⁾. The database is also publicly available on CasJobs ²⁾. Luo et al. [25]³⁾ introduced the survey design, the observational and instrumental limitations, data reduction and analysis of LAMOST. The spectral type and basic parameters of the co-added spectra were derived by LAMOST stellar parameter pipeline [26]. Among all the spectra published in DR5, about six million spectra were assigned with effective temperatures, metallicities, surface gravities, heliocentric radial velocities, and errors. Multi-epoch radial velocity measurements are helpful in studying the physics of binary systems. For instance, Qian et al. [27] presented $\sim 256,000$ spectroscopic binary or variable candidates with radial velocity variation $\Delta V_R > 10 \text{ km s}^{-1}$. Gao et al. [28] estimated the fraction of binary stars by repeating spectral observations from LAMOST. Yi, Sun & Gu [29] predicted around 400 BH binary candidates could be found by the LAMOST surveys. Recently, for binaries with unknown orbital periods, Gu et al. [30] proposed a method to search for stellar-mass BH candidates with giant companions from spectroscopic observations. For binaries with known orbital periods, Zheng et al. [31] showed that the mass of an optically invisible object in the binary can be well-constrained. Since only co-added spectrum on the same observation night was released in LAMOST DR5, the identified binary systems usually have a longer orbital period (> 1 day). Recently, Bai et al. [32] released corresponding single-epoch data of all sources in LAMOST DR5 general catalog (hereafter DR5GC). They presented the first data release of LAMOST low-resolution single-epoch spectra ⁴⁾, typically not less than three exposures at each observation night. Their catalog was perfectly suitable to study close binaries, in particular, to search for spectroscopic binaries in short orbital periods (< 1 day) using radial velocity methods. Close binary candidates based on the database from Bai et al. [32] would be available at Yuan et al. (in preparation). We can search for compact object candidates with short periods (< 1 day) based on V_R from Bai et al. [32]. Moreover, these binaries are more accessible to follow-up dynamical measurement with spectroscopic observations.

This study focuses on the close binary comprising a compact object and a K/M-dwarf companion from the single-lined spectroscopic binaries of DR5GC. The rest of this study is organized as follows. The sample and data analyses are presented in

1) See <http://dr5.lamost.org/>

2) See <http://sdss.china-vo.org/casjobs/>

3) see <http://www.lamost.org/public/dr/algorithms/spectra-anlyse?locale=en>

4) see <http://dr5.lamost.org/sedr5/>

sect. 2. The results are presented in sect. 3. Summary and discussion are presented in sect. 4.

2 Sample and Analyses

The catalog of single-lined spectroscopic binaries with multi-epoch observations was presented by Bai et al. [32]. A series of frequently-used lines (refer to Table 1 of [32]) were selected to calculate V_R . The wavelength bands used to calculate K/M-dwarfs are 4550-5300 Å and 6350-9000 Å. V_R was measured by minimizing χ^2 between the spectrum and its best template. V_R can be well-estimated from spectroscopic observations with the signal-to-noise ratio $S/N > 10$ [32]. Based on the catalog of Bai et al. [32], binaries with K/M-dwarf companions are selected by containing repeated radial velocity measurements (at least three times) within 3". In this study, we select candidates according to the following criteria:

- (i) signal-to-noise ratio $S/N > 10$ is required in the g -band;
- (ii) single-lined spectroscopic binary systems only;
- (iii) large radial velocity variation $\Delta V_R > 150 \text{ km s}^{-1}$;
- (iv) spectral type classified as K/M-dwarfs;
- (v) not eclipsing binaries.

Although the initial cut of criteria (i-iii) is effective at excluding binaries with small V_R variations, some bad V_R measurements still remained. Thus, we visually inspect each spectrum by reexamining the profile (single peak) and center position (V_R) of the major lines in K/M-dwarfs, e.g., $H\alpha$ and $H\beta$. Spectra which characterized double-lined features or poorly measured radial velocities are ruled out. In a single-lined spectroscopic binary, an optically visible star and unseen object are denoted as M_1 and M_2 , respectively. There are two possibilities for the object M_2 : (I), an MS star with relatively low mass and luminosity (empirically, for $L_2/L_1 \lesssim 1/10$ or equivalently, $M_2/M_1 \lesssim 1/2$); (II), a compact object (WD, NS, or BH).

There are two reasons for choosing K/M-dwarfs. First, K/M-dwarfs have a relatively low mass and thus generally have large Keplerian velocity in close binaries. Since the average uncertainty of the radial velocity measurements is approximately 5 km s^{-1} [24] in the low-resolution spectra, larger radial velocity variations will reduce the relative uncertainty for good constraints in our analyses. Second, whether the unseen object is a compact candidate or a dimmer dwarf is much more easily distinguished due to the larger discrepancy between the masses for these two object types. Namely, an MS star with relatively low mass and luminosity is far lighter than a BH or an NS. Hence, it is much easier to identify the unseen object from the amplitude of radial velocity variation. There are 308 binaries meet the criteria (i-iii) in total. The sample has been narrowed down to 81 single-lined binaries with K/M-dwarf companions after imposing constraints (i-iv). We cross-match the 308 sources with Gaia early data release 3 (Gaia EDR3) [33] using a matching radius of 3". G-band magnitude and median $BP - RP$ color were adopted from Gaia EDR3. The G-band extinction is taken into account. Figure 1 shows the locations of 308 sources in the color-magnitude diagram. It is seen that the sources in our sample are confined to the MS.

Since the Transiting Exoplanet Survey Satellite (TESS [34])⁵⁾ is optimized to observe low-mass stars that potentially harbor exoplanets, it is a perfect cross-match with the sample of K/M-dwarfs in this study. We implement high cadence photometry from the TESS to exclude contaminations such as eclipsing binaries and search for periods of the candidate sources. We use the open-source tool, *eleanor*, to extract TESS light curves [34, 35]. The target pixel files (15×15 pixels) were cut out from the TESS full-frame images. We remove flux data that were distributed outside of 3σ and flux with large error bars (top 5%). The period was searched by using the generalized Lomb-Scargle periodogram [36, 37]. We visually inspect each light curve to exclude 25 eclipsing binaries. There are 19 sources that show ellipsoidal modulation [38, 39] effects, i.e., the light curve features a quasi-sinusoidal shape due to the rotation of the tidally distorted star. Light curves are presented in the Figures S1 and S2 of [Supplementary Material](#), respectively. Interestingly, some of the ellipsoidal light curves show a certain degree of asymmetry between the two maxima, which could originate from some unknown orbital modulations rather than the pure ellipsoidal. This phenomenon is called the O'Connell effect [40]. Traditionally, these asymmetries are often thought to be explained by models of dark spots [41-44], hot spots [45, 46], or magnetohydrodynamics [47], which are beyond the scope of this paper. In addition,

5) See <https://mast.stsci.edu/portal/Mashup/Clients/Mast/Portal.html>

there are 37 sources with no significant photometric periodicity, which require further analyses from the theoretical perspective (see below).

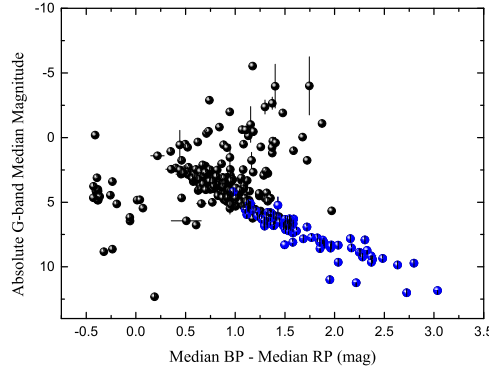


Figure 1 Comparison of 81 K/M-dwarf binaries (blue circles: the criteria i-iv) and the total 308 binaries (all circles: the criteria i-iii) in a color-magnitude diagram.

For simplicity, we assume a circular orbit (eccentricity $e = 0$). The mass function for the invisible object [5] is

$$f(m_2) = \frac{m_2^3 \sin^3 i}{(m_1 + m_2)^2} = 1.0361 \times 10^{-7} \left(\frac{K_1}{\text{km s}^{-1}} \right)^3 \frac{P_{\text{orb}}}{\text{days}}, \quad (1)$$

where $m_1 = M_1/M_\odot$ and $m_2 = M_2/M_\odot$ are dimensionless masses (M_\odot being the solar mass), i is the inclination angle of the orbit, K_1 is the semi-amplitude of radial velocity curve (in km s^{-1}), and P_{orb} is the orbital period (in days). If the object M_2 is a low-mass MS star, i.e., $M_2 \lesssim M_1/2$. Then, we can obtain the following constraint for K_1 based on Eq. (1):

$$K_1 \lesssim 81.24 \left(\frac{m_1}{P_{\text{orb}}/\text{days}} \right)^{1/3} \text{ km s}^{-1}. \quad (2)$$

Obviously, $\Delta V_R/2$ can be regarded as the lower limit of the semi-amplitude K_1 , i.e., $K_1 \geq \Delta V_R/2$, where ΔV_R is the largest variation between all radial velocity measurements for a specific source. Then, we can derive the following constraint,

$$\frac{\Delta V_R}{2} \lesssim 81.24 \left(\frac{m_1}{P_{\text{orb}}/\text{days}} \right)^{1/3} \text{ km s}^{-1}. \quad (3)$$

Eq. (3) shows the upper limit for the radial velocity variation for Case (I), i.e., a much fainter MS star. Thus, if M_1 and P_{orb} are derived from the optical observations, and the radial velocity variation is beyond the upper limit, then the unseen object can be regarded as a compact object candidate.

For 37 sources with no significant photometric periodicity, a strict lower limit of orbital period $P_{\text{orb}}^{\text{min}}$ is evaluated as follows. Based on the assumption that the Roche-lobe radius is not less than the radius of the K/M-dwarf, i.e., $R_{L1} \geq R_1$ [30], there exists a lower limit for the orbital period [31]:

$$P_{\text{orb}}^{\text{min}} = 0.369(\rho_1/\rho_\odot)^{-1/2} \text{ days}, \quad (4)$$

where ρ_\odot is the solar density. Thus, $P_{\text{orb}}^{\text{min}}$ simply depends on the mass density ρ_1 . The mass-radius relation (MRR) for the low mass ($M_1 < 1.66M_\odot$) MS stars takes the form [48]:

$$r_1 = 1.06m_1^{0.945}, \quad (5)$$

where $r_1 = R_1/R_\odot$. By combining eqs. (4) and (5), we obtain

$$P_{\text{orb}}^{\text{min}} = 0.403m_1^{0.9175} \text{ days}. \quad (6)$$

To evaluate $P_{\text{orb}}^{\text{min}}$, the mass M_1 should be estimated in advance. We estimated M_1 by using an empirical mass-luminosity relation [49], where M_K is the absolute magnitude in the K-band (infrared between 2 and 3 micron) from 2MASS [50].

3 Results

A comparison of the observations with the theoretical line (eq. (3)) in $\Delta V_R/2 - P_{\text{orb}}$ diagram is shown in Figure 2. Here, we adopt a median value $M_1 = 0.8M_\odot$, with a range of $0.6 - 1.0M_\odot$ for K-dwarfs; and a median value $M_1 = 0.4M_\odot$, with a range of $0.2 - 0.6M_\odot$ for M-dwarfs. We also plot a few dynamically confirmed BHs with short orbital periods simply for comparison (black circles in Figure 2); data were adopted from the catalog of Corral-Santana et al. [8] and Tetarenko et al. [9].

Owing to the insufficient cadence of observations [30,31], $\Delta V_R/2$ is a lower limit of the semi-amplitude of the radial velocity curve. For the sources located below the theoretical lines, they could not be selected as candidates of the compact objects for now. 11 K-dwarfs locate in (or above) the $0.6 - 1.0M_\odot$ region, and 24 M-dwarfs locate in (or above) the $0.2 - 0.6M_\odot$ region. The parameters for the 35 sources are shown in Table 1. The combined spectra of the 35 sources are presented in the Figure S3. We fit the spectra of the 35 sources using a mixture of stellar models provided by the PyHammer package [51]. PyHammer has introduced in its version 2 [52], a fully automatic technique to spectral type spectroscopic binaries. We find that 20 sources are well-fitted by a single star template, whereas 15 sources could be fitted with combined templates of WD+K/M-dwarf (the classification results are presented in the last column of Table 1). Our test shows that the sample is not contaminated by binary stars. According to the theoretical analyses in sect. 2, the unseen object M_2 of the 35 sources is unlikely to be a much fainter MS star with low mass and low luminosity. Instead, M_2 could be regarded as a compact object candidate. The astrometric parallax and the total proper motion from Gaia EDR3 [33] are also presented in Table 1. We collect Gaia astrometric quality flags. *ruwe* (the renormalised unit weight error), *astrometric_excess_noise* (excess noise of the source) and *phot_bp_rp_excess_factor* (BP/RP flux excess factor) are added in the Table S1 of the [Supplementary Material](#).

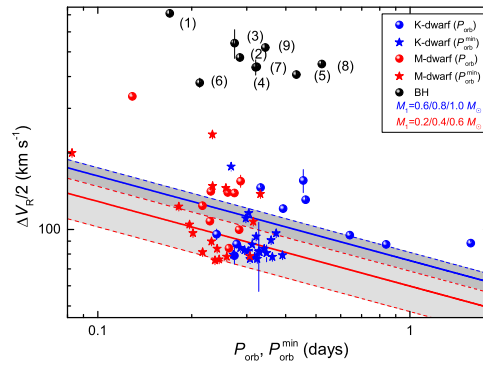


Figure 2 Comparison of the observations (circles) with the theoretical results (lines) in the $\Delta V_R/2 - P_{\text{orb}}$ diagram. The blue and red circles represent K- and M-dwarfs, respectively. The blue and red solid lines represent the theoretical upper limits (eq. (3)) with a median mass $M_1 = 0.8M_\odot$ for K-dwarfs and $M_1 = 0.4M_\odot$ for M-dwarfs, respectively. The gray region ($0.6 - 1.0M_\odot$) and the light gray region ($0.2 - 0.6M_\odot$) are typical mass ranges for K- and M-dwarfs, respectively. The black circles represent known BHBs with MS companions: (1) XTE J1118+480; (2) GRS 1009-45; (3) XTE J1859+226; (4) XTE J1650-500; (5) GS 1124-684; (6) GRO J0422+32; (7) 3A 0620-003; (8) H 1705-250; (9) GS 2000+251.

The inclination angle is also expected to be smaller than 90° by assuming a certain distribution (not random though, due to the selection effects) of the orientations of orbital planes. To fully solve the orbital parameters of the systems, more follow-up observations should be conducted, and the candidates of compact objects should be solidly confirmed. The reasoning also holds for the sources above the theoretical lines. Minimum mass functions (assume $K = \Delta V_R/2$ and $P_{\text{orb}} = P$ or $P_{\text{orb}}^{\text{min}}$) are shown in Table 2. Moreover, the estimated mass of the K/M-dwarf companions M_1 and the unseen objects M_2 are presented in Table 2, where six uniform inclinations in sine ($\sin i = 1, 0.9, 0.8, 0.7, 0.6$ and 0.5) are considered.

As mentioned in the selection process, we have excluded apparent eclipsing binaries. We cross-matched our sources with SIMBAD Database ⁶⁾ using a matching radius of $3''$. Several sources in our sample were previously known as the EB*WUMa type, as denoted in the last column in Table 1. However, the following argument shows that at least some sources may not be eclipsing binaries. No.5 and No.7 serve as two examples for more detailed analyses. The targets' observation log is shown in Table 3. Using the orbital period from the light curve, we folded and fitted the radial velocity data with a sinusoidal function: $V_R = K_1 \sin(2\pi/P_{\text{orb}}(t - t_0)) + V_0$, where K_1 is the radial velocity curve semi-amplitude, t_0 is an epoch at orbital phase 0, and

⁶⁾ See <http://simbad.u-strasbg.fr/simbad/>

V_0 is the radial velocity of the system's center of mass (with respect to the Earth). Figure 3 shows the phase-folded light curve (upper panels) and the best-fitted radial velocity curve (lower panels). The semi-amplitude $K_1 = 195 \pm 28 \text{ km s}^{-1}$ (No.5) and $158 \pm 2 \text{ km s}^{-1}$ (No.7), which is larger than the radial velocity variation $\Delta V_R/2 = 124 \pm 4 \text{ km s}^{-1}$ (No.5) and $156 \pm 17 \text{ km s}^{-1}$ (No.7) measured by the single-epoch spectra. The corresponding mass functions of the two sources are $f(m_2) \sim 0.18 M_\odot$ (No.5) and $0.19 M_\odot$ (No.7), respectively. For $M_1 \sim 0.60 - 0.65 M_\odot$, M_2 is derived as $M_2 \sim 0.70 - 0.75 M_\odot$, which is always higher than M_1 . M_2 under typical inclination angles are also shown in Figure 4. Thus, M_2 may be regarded as a compact object candidate, and the system is unlikely an eclipsing binary of the EB*WUMa type.

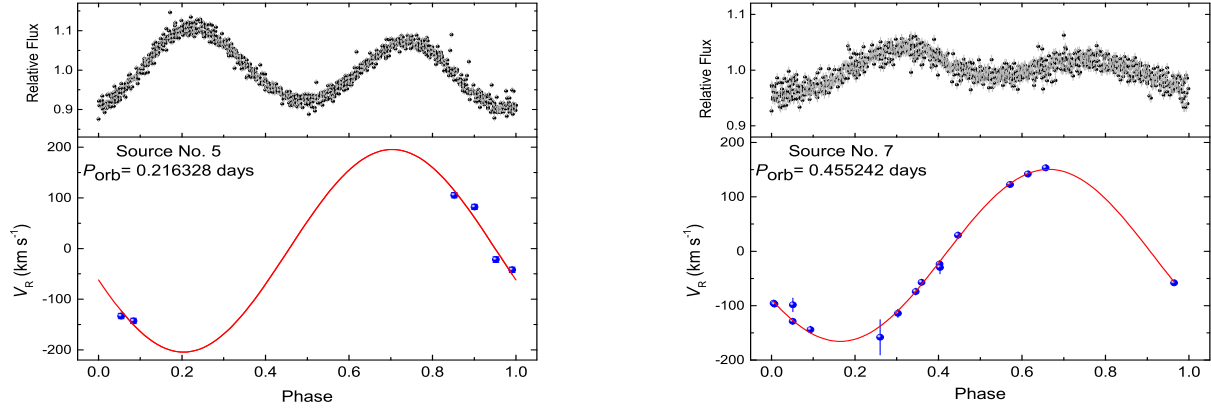


Figure 3 V-mag light curve and radial velocity curve of the example sources (No.5 and No.7). Upper panel: the folded TESS light curve with the orbital period derived from the Lomb-Scargle periodogram. Lower panel: radial velocities (black dots; some error bars are too small to be seen) and the best-fitted radial velocity curve (red curve).

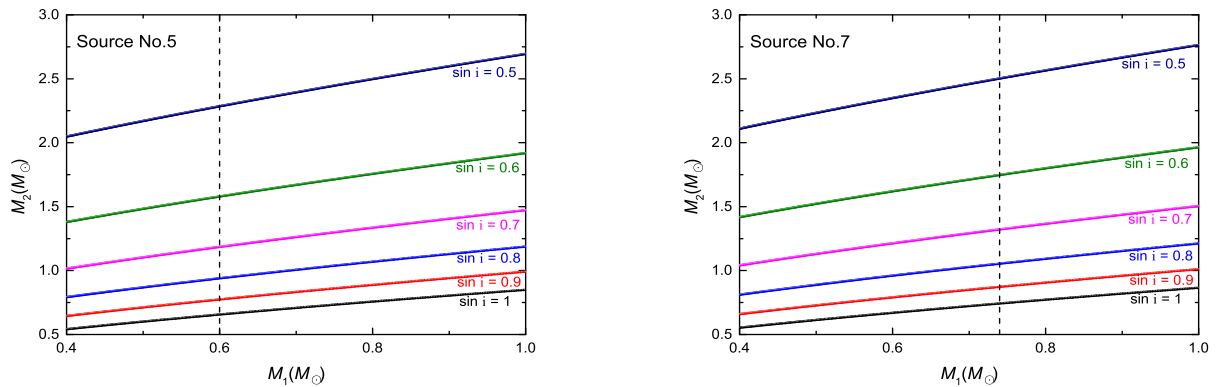


Figure 4 By the results of radial velocity curve fitting, the comparison of M_2 with M_1 about the two examples (No.5 and No.7). Six values of the orbital inclination from $\sin i = 1.0$ to 0.5 were considered. The vertical dashed line represents the M_1 estimated by the empirical mass-luminosity relation.

In addition, a short comment on three other systems in our sample is presented. Notably, No.10 [53], No.18 [54] and No.30 [20] were previously identified as WD+M-dwarf eclipsing binaries systems, which were re-discovered by our selection procedures. It is seen from Figure S3 that, No.10 and No.30 are obviously WD+M-dwarfs. No.2 was identified as (1) an X-ray source according to Chandra's observation; (2) a UV-excess star cataloged in Bai et al. [55], which indicate that the source could be an accreting system with a visible star filling the Roche lobe. In addition, a recent study on source No.11, proposed that the system contains an NS or an unusually high-mass WD, by utilizing the spectroscopy of LAMOST and Palomar 200-inch telescope, and the high-cadence photometry of TESS (Yi, Gu, Zhang et al., under review).

4 Summary and Discussion

In this study, we have focused on the compact object candidates in close binaries with K/M-dwarf companions. For the case that the unseen object in the binary is an MS star with lower luminosity, we have obtained an upper limit for the semi-amplitude of radial velocity variation (eq. (3)). In other words, if the radial velocity variation derived from the LAMOST spectra is beyond the upper limit, the unseen object can be regarded as a compact object candidate. We have derived 35 compact object candidates, by using only the limited exposures from LAMOST low-resolution survey, aided with photometric light curves. This study demonstrates the principle and power of searching for compact objects through LAMOST low-resolution survey.

Notably, majority of K/M binaries, including those with compact companions, likely have long periods. The systems are harder to detect because the induced V_R variations are smaller. Thus the systems are not investigated in the current work. Candidates in our sample need more careful analysis, e.g., contaminations from subtle double-line spectroscopic binaries (e.g., equal mass pairs), the inaccurate estimation of mass or stellar parameters, the case of triple systems, or higher-order multiples. For instance, trying to exclude spectroscopic binaries through visual inspection and PyHammer [51, 52] could not provide a quantitative estimation of the false classification rate. A more rigorous approach to exclude contaminations should be similar to the spectral fitting of El-Badry et al. [56]. However, since the resolution and signal-to-noise ratio of the spectra used in this study is relatively low, it is difficult to give a very precise classification. Therefore, some candidates in our sample might be spectroscopic binaries. These problems can be improved in future works, for instance, using the higher-resolution spectroscopy from LAMOST medium-resolution survey ($R \sim 7500$) [57] and the SDSS APOGEE data ($R \sim 22000$).

Recently, Shao et al. [58] simulated the Galactic population of detached BH binaries with normal-star companions. They showed that it is difficult for conventional models to produce BH low-mass XRBs. However, some investigations of massive star evolution suggested that the BH progenitors have masses as low as $\sim 15M_{\odot}$ [59]. Based on such a result, Shao et al. [58] showed that the overall population of detached BH binaries is dominated by those with relatively low-mass companions. Shao et al. [58] also predicted that the total number of detached BH binaries with MS companions is more than 4,000, among which 700 systems have companions brighter than 20 mag. In this spirit, the compact object candidates in our sample are worth follow-up observations for precise dynamical measurement.

Despite using the spectroscopic and photometric data from surveys, astrometric surveys can also be used to search for compact objects in binary systems. For instance, Gandhi et al. [60] proposed a method of using the astrometric excess noise, to discover candidate X-ray emitting sources (accreting binaries). The newly released data (EDR3) of Gaia ⁷⁾ will present an unprecedented opportunity for compact object searching tasks. A joined study of data from Gaia, LAMOST, and various photometric surveys can extend the capability of discoveries.

This work was supported by the National Natural Science Foundation of China (NSFC) under grants 12103047, 11925301, 12033006, and 12005192, and the National Key Research and Development Program of China (2019YFA0405000). We acknowledge the science research grants from the China Manned Space Project with NO. CMS-CSST-2021-B07, acknowledge support from the Project funded by China Postdoctoral Science Foundation under grants 2019TQ0288, 2020TQ0287, and 2020M672255, and 2021M702742. and acknowledge the Natural Science Foundation of Henan Province of China 212300410290. This work has made use of data products from the Guoshoujing Telescope (the Large Sky Area Multi-Object Fiber Spectroscopic Telescope, LAMOST). LAMOST is a National Major Scientific Project built by the Chinese Academy of Sciences. Funding for the project has been provided by the National Development and Reform Commission. LAMOST is operated and managed by the National Astronomical Observatories, Chinese Academy of Sciences. We acknowledge the use of public TESS data from pipelines at the TESS Science Office and at the TESS Science Processing Operations Center. We thank Yi-Ze Dong, Yu Bai, Fan Yang, Mou-Yuan Sun, and Jin-Bo Fu for beneficial discussions during the derivation of our sample, and thank the referee for helpful suggestions that improved the manuscript.

Conflict of interest The authors declare that they have no conflict of interest.

- 1 Patterson, J., *Astrophys. J. Suppl. Ser.* **54**, 443 (1984).
- 2 Joss, P. C. & Rappaport, S. A., *Annu. Rev. Astron. Astrophys.* **22**, 537 (1984).
- 3 Ritter, H. & Kolb, U., *Astron. & Astrophys.* **404**, 301 (2003).
- 4 Warner, B., *Cataclysmic Variable Stars*, Cambridge University Press, pp. 592 (2003).
- 5 Remillard, R. A., & McClintock, J. E., *Annu. Rev. Astron. Astrophys.* **44**, 49 (2006).
- 6 McClintock, J. E. & Remillard, R. A., *Compact stellar X-ray sources*, 157 (2006).
- 7 Casares, J., & Jonker, P. G., *Space. Sci. Rev.* **183**, 223 (2014).
- 8 Corral-Santana, J. M., Casares, J., Muñoz-Darias, T., et al., *Astron. & Astrophys.* **587**, A61 (2016).
- 9 Tetarenko, B. E., Sivakoff, G. R., Heinke, C. O., & Gladstone, J. C., *Astrophys. J. Suppl. Ser.* **222**, 15 (2016).
- 10 Thompson, T. A., Kochanek, C. S., Stanek, K. Z., et al., *Sci.*, **366**, 637 (2019).

7) <https://www.cosmos.esa.int/web/gaia/early-data-release-3>

- 11 Liu, J., Zhang, H., Howard, A. W., et al., *Natur.*, **575**, 618 (2019).
- 12 Price-Whelan, A. M., Hogg, D. W., Rix, H.-W., et al., *Astrophys. J.* 895, 2 (2020).
- 13 Rowan, D. M., Stanek, K. Z., Jayasinghe, T., et al., *Mon. Notic. Roy. Astron. Soc.*, 507, 104 (2021).
- 14 Pyrzas, S., Gänsicke, B. T., Marsh, T. R., et al., *Mon. Notic. Roy. Astron. Soc.* **394**, 978 (2009).
- 15 Bradt, H. V. D., & McClintock, J. E. *Annu. Rev. Astron. Astrophys.* **21**, 13 (1983).
- 16 van Paradijs, J., & McClintock, J. E. *X-ray Binaries*, **58** (1995).
- 17 Liu, Q. Z., van Paradijs, J., & van den Heuvel, E. P. J., *Astron. & Astrophys.* **455**, 1165 (2006).
- 18 Liu, Q. Z., van Paradijs, J., & van den Heuvel, E. P. J., *Astron. & Astrophys.* **469**, 807 (2007).
- 19 Rebassa-Mansergas, A., Ren, J. J., Parsons, S. G., et al., *Mon. Notic. Roy. Astron. Soc.* **458**, 3808 (2016).
- 20 Ren, J.-J., Rebassa-Mansergas, A., Parsons, S. G., et al., *Mon. Notic. Roy. Astron. Soc.* **477**, 4641 (2018).
- 21 Wang, S.-G., Su, D.-Q., Chu, Y.-Q., Cui, X., & Wang, Y.-N., *Appl. Opt.*, **35**, 5155 (1996).
- 22 Su, D.-Q., & Cui, X.-Q., *Chin. J. Astron. & Astrophys.*, **4**, 1 (2004).
- 23 Cui, X.-Q., Zhao, Y.-H., Chu, Y.-Q., et al., *Res. Astron. Astrophys.* **12**, 1197 (2012).
- 24 Deng, L.-C., Newberg, H. J., Liu, C., et al., *Res. Astron. Astrophys.* **12**, 735 (2012).
- 25 Luo, A.-L., Zhao, Y.-H., Zhao, G., et al., *Res. Astron. Astrophys.* **15**, 1095 (2015).
- 26 Wu, Y., Luo, A.-L., Li, H.-N., et al., *Res. Astron. Astrophys.* **11**, 924 (2011).
- 27 Qian, S.-B., Shi, X.-D., Zhu, L.-Y., et al., *Res. Astron. Astrophys.* **19**, 064 (2019).
- 28 Gao, S., Zhao, H., Yang, H., et al., *Mon. Notic. Roy. Astron. Soc.* 469, L68 (2017).
- 29 Yi, T., Sun, M., & Gu, W.-M., *Astrophys. J.* **886**, 97 (2019).
- 30 Gu, W.-M., Mu, H.-J., Fu, J.-B., et al., *Astrophys. J. Lett.* **872**, L20 (2019).
- 31 Zheng, L.-L., Gu, W.-M., Yi, T., et al., *Astron J.*, **158**, 179 (2019).
- 32 Bai, Z.-R., Zhang, H.-T., Yuan, H.-L., et al. 2021, arXiv:2106.12715
- 33 Gaia Collaboration 2020, *VizieR Online Data Catalog*, I/350 (2020).
- 34 Ricker, G. R., Winn, J. N., Vanderspek, R., et al., *J. Astron. Telesc. Instrum. Syst.*, **1**, 014003 (2015).
- 35 Feinstein, A. D., Montet, B. T., Foreman-Mackey, D., et al., *Publ. Astron. Soc. Pac.* **131**, 094502 (2019).
- 36 Scargle, J. D., *Astrophys. J.* **263**, 835 (1982).
- 37 Zechmeister, M., & Kürster, M., *Astron. & Astrophys.* **496**, 577 (2009).
- 38 Morris, S. L., *Astrophys. J.*, 295, 143 (1985).
- 39 Morris, S. L. & Naftilan, S. A., *Astrophys. J.*, 419, 344 (1993).
- 40 O'Connell, D. J. K., *Publications of the Riverview College Observatory*, **2**, 85 (1951).
- 41 Bopp, B. W. & Noah, P. V., *Publ Astron Soc Pac.*, **92**, 717 (1980).
- 42 Broens, E., *Mon. Notic. Roy. Astron. Soc.*, 430, 3070 (2013).
- 43 Li, K., Qian, S.-B., Hu, S.-M., et al., *Astron J.*, 147, 98 (2014).
- 44 Li, K., Hu, S., Guo, D., et al., *NewA*, **41**, 17 (2015).
- 45 Soonthornthum, B., Aungwerojwit, A., Yang, Y., et al., *Astrophysics and Space Science Library*, **298**, Li (2003).
- 46 Virnina, N. A., *Open European Journal on Variable Stars*, **139**, 20 (2011).
- 47 McCartney, S. A., *Ph.D. Thesis*, 5565 (1999).
- 48 Demircan, O., & Kahraman, G., *Astrophys. Space. Sci.* **181**, 313 (1991).
- 49 Henry, T. J. & McCarthy, D. W., *Astron J.*, 106, 773 (1993).
- 50 Cutri, R. M., Skrutskie, M. F., van Dyk, S., et al., *VizieR Online Data Catalog*, II/246 (2003).
- 51 Kesseli, A. Y., West, A. A., Veyette, M., et al., *Astrophys. J. Suppl. Ser.*, **230**, 16 (2017).
- 52 Roulston, B. R., Green, P. J., & Kesseli, A. Y., *Astrophys. J. Suppl. Ser.*, **249**, 34 (2020).
- 53 Parsons, S. G., Agurto-Gangas, C., Gänsicke, B. T., et al., *Mon. Notic. Roy. Astron. Soc.*, **449**, 2194 (2015).
- 54 Law, N. M., Kraus, A. L., Street, R., et al., *Astrophys. J.* **757**, 133 (2012).
- 55 Bai, Y., Liu, J., Wicker, J., et al., *Astrophys. J. Suppl. Ser.* **235**, 16 (2018).
- 56 El-Badry, K., Rix, H.-W., Ting, Y.-S., et al., *Mon. Notic. Roy. Astron. Soc.*, 473, 5043 (2018).
- 57 Liu, C., Fu, J., Shi, J., et al., arXiv:2005.0721 (2020).
- 58 Shao, Y., & Li, X.-D., *Astrophys. J.* **885**, 151 (2019).
- 59 Sukhbold, T., Ertl, T., Woosley, S. E., et al., *Astrophys. J.* **821**, 38 (2016).
- 60 Gandhi, P., Buckley, D. A. H., Charles, P., et al., arXiv:2009.07277 (2020).

Table 1 Parameters for the compact object candidates with K/M-dwarf companions.

No.	Designation	Type1	T_{eff} (K)	ϖ (mas)	pm (mas/yr)	ΔV_R (km s ⁻¹)	P_{orb} or $P_{\text{orb}}^{\text{min}}$ (days)	Type2	Type3
a)	b)	c)	d)	e)	f)	g)	h)	i)	j)
(1)	J013008.78+360226.7	M3	3133 ±69	23.426 ±0.039	42.712 ±0.042	169 ±1	0.2631	–	M6
(2)	J013622.94+210017.9	M0	3740 ±68	5.868 ±0.021	6.589 ±0.031	282 ±2	0.2300	EB*	M1
(3)	J045242.82+122006.9	K7	3994 ±98	5.935 ±0.020	32.738 ±0.030	292 ±2	0.3322	–	K4+DA1.5
(4)	J063656.98+412931.3	M0	3861 ±84	2.695 ±0.055	40.761 ±0.065	279 ±6	0.2605	EB*	K7+DA2.0
(5)	J070307.60+344203.3	M0	3707 ±74	4.735 ±0.030	13.140 ±0.041	248 ±3	0.2163	ELL	M2
(6)	J072710.26+341730.1	M0	3800 ±83	2.051 ±0.070	38.905 ±0.097	215 ±5	0.2286	EB*	M2+DA5.0
(7)	J074432.30+395421.5	K3	4647 ±56	2.033 ±0.030	20.152 ±0.044	312 ±32	0.4552	EB*	K3+dCK
(8)	J091631.61+271614.7	M2	3632 ±70	3.793 ±0.071	22.269 ±0.087	310 ±17	0.2865	–	M4
(9)	J094653.67+535754.0	K7	5316 ±151	4.050 ±0.022	22.338 ±0.028	174 ±2	0.8382	–	K2
(10)	J101356.31+272410.8	M3	3504 ±89	7.469 ±0.064	57.903 ±0.082	668 ±8	0.1290	WD+M4	M4+DA5.5
(11)	J112306.94+400736.7	M0	3682 ±74	3.147 ±0.038	31.841 ±0.050	278 ±3	0.2738	EB*	M2
(12)	J113713.64+124559.9	K4	4485 ±82	3.179 ±0.020	6.578 ±0.025	190 ±3	0.6410	–	K4
(13)	J115059.18+272806.0	M2	3700 ±79	4.896 ±0.044	17.589 ±0.062	199 ±3	0.2838	–	M3
(14)	J120802.64+311103.9	K3	4670 ±29	11.251 ±0.019	80.843 ±0.028	262 ±0	0.4630	RotV*	K3+dCK
(15)	J121046.90+303403.2	K5	4478 ±53	1.962 ±0.034	15.931 ±0.045	242 ±7	0.3922	EB*	K4+DA1.5
(16)	J150335.90+224322.7	K3	4916 ±105	1.437 ±0.029	11.965 ±0.039	177 ±2	1.5643	–	K2+dCK
(17)	J002909.24+361323.8	M0	3873 ±77	2.938 ±0.053	30.568 ±0.062	168 ±3	0.2411	–	M0
(18)	J015256.57+384413.4	M3	3673 ±77	4.354 ±0.055	23.633 ±0.094	209 ±3	0.1968	WD+M3	M4
(19)	J035540.77+381549.9	M3	3323 ±79	4.644 ±0.063	50.630 ±0.082	163 ±2	0.2167	–	M5
(20)	J035916.33+400732.3	M0	3691 ±80	2.900 ±0.063	5.661 ±0.099	152 ±4	0.2447	–	M2+DA3.5
(21)	J041004.94+293102.0	M0	3833 ±108	6.485 ±0.050	36.240 ±0.072	215 ±5	0.3148	EB*	M0
(22)	J041116.70+221522.4	M0	3814 ±70	5.641 ±0.023	71.823 ±0.033	275 ±2	0.3315	–	K7+DA2.0
(23)	J050854.93+303039.0	K7	3796 ±90	2.249 ±0.062	7.299 ±0.094	353 ±13	0.2675	–	K7+DA0.5
(24)	J060253.72+003558.4	M2	3612 ±78	8.501 ±0.026	21.402 ±0.036	473 ±2	0.2329	–	M3
(25)	J060418.87+250218.8	K7	4228 ±139	1.222 ±0.076	4.955 ±0.110	232 ±7	0.3044	–	K3+DA1.5
(26)	J063023.56+210952.8	M0	3758 ±73	4.621 ±0.033	25.715 ±0.041	291 ±2	0.2572	–	M0+DA2.5
(27)	J072225.45+220525.8	M3	3386 ±83	6.671 ±0.042	71.308 ±0.057	246 ±3	0.1819	–	M6
(28)	J081035.34+230444.9	M2	3664 ±91	3.537 ±0.051	14.391 ±0.067	179 ±4	0.2314	–	M3
(29)	J090826.14+123648.2	M6	3100 ±76	20.474 ±0.037	204.311 ±0.049	400 ±2	0.0827	EB*	M6
(30)	J093507.99+270049.2	M4	3443 ±78	5.252 ±0.048	26.204 ±0.064	193 ±2	0.2019	ELL	M6+DA6.5
(31)	J093524.14+110836.2	K0	5149 ±217	1.1207±0.0478	15.213±0.065	193 ±3	0.3726	EB*	K2
(32)	J094811.23+552728.2	M0	3858 ±90	1.326 ±0.058	8.851 ±0.075	157 ±5	0.3069	–	M1
(33)	J104444.64+190229.6	K7	4143 ±145	2.344 ±0.032	22.607 ±0.052	221 ±4	0.2978	–	K4+DA1.0
(34)	J104531.95+582901.5	M2	3657 ±85	2.862 ±0.049	14.964 ±0.056	296 ±3	0.2331	–	M4
(35)	J161922.13+081914.3	M0	3867 ±67	4.158 ±0.027	41.474 ±0.034	156 ±2	0.2589	–	M0

* a) The serial number of the sources. b) Target designation. c) Spectral types reported by LAMOST. We adopt the spectral type in this column throughout the paper to report the number of K/M dwarfs. d) The effective temperature. e) The parallax from Gaia EDR3. f) The total proper motion from Gaia EDR3. g) The largest variation of radial velocity measurement from the single epoch spectra of LAMOST. h) The orbital period P_{orb} of the binaries No. (1-16). $P_{\text{orb}}^{\text{min}}$ is adopted for the sources No. (17-35). i) The main type of the source from the SIMBAD Database. EB, ELL, and RotV represent eclipsing binary, ellipsoidal variable star, and rotational variable star, respectively. j) The spectral type from PyHammer classification.

Table 2 Evaluation of M_2 for the compact object candidates in our sample.

No.	Designation	f_{\min}	M_1	$M_{2,\sin i=1}$	$M_{2,\sin i=0.9}$	$M_{2,\sin i=0.8}$	$M_{2,\sin i=0.7}$	$M_{2,\sin i=0.6}$	$M_{2,\sin i=0.5}$
a)	b)	c)	d)	e)	f)	g)	h)	i)	j)
(1)	J013008.78+360226.7	0.02	0.18	0.11	0.13	0.15	0.18	0.23	0.32
(2)	J013622.94+210017.9	0.07	0.63	0.42	0.48	0.57	0.70	0.90	1.23
(3)	J045242.82+122006.9	0.08	0.68	0.47	0.54	0.64	0.79	1.01	1.39
(4)	J063656.98+412931.3	0.07	0.66	0.45	0.52	0.62	0.75	0.96	1.32
(5)	J070307.60+344203.3	0.04	0.60	0.34	0.39	0.45	0.55	0.69	0.93
(6)	J072710.26+341730.1	0.03	0.58	0.28	0.32	0.37	0.45	0.56	0.74
(7)	J074432.30+395421.5	0.18	0.74	0.73	0.85	1.03	1.29	1.70	2.43
(8)	J091631.61+271614.7	0.11	0.50	0.47	0.55	0.66	0.83	1.09	1.54
(9)	J094653.67+535754.0	0.06	0.42	0.32	0.37	0.44	0.54	0.69	0.96
(10)	J101356.31+272410.8	0.50	0.23	0.81	1.02	1.33	1.83	2.71	4.40
(11)	J112306.94+400736.7	0.08	0.60	0.43	0.50	0.60	0.74	0.95	1.31
(12)	J113713.64+124559.9	0.06	0.78	0.44	0.50	0.59	0.72	0.91	1.22
(13)	J115059.18+272806.0	0.03	0.51	0.26	0.30	0.35	0.42	0.52	0.70
(14)	J120802.64+311103.9	0.11	0.74	0.57	0.66	0.79	0.97	1.26	1.75
(15)	J121046.90+303403.2	0.07	0.80	0.49	0.57	0.67	0.82	1.04	1.41
(16)	J150335.90+224322.7	0.11	0.86	0.63	0.73	0.87	1.06	1.37	1.89
(17)	J002909.24+361323.8	0.01	0.57	0.21	0.24	0.27	0.33	0.40	0.52
(18)	J015256.57+384413.4	0.02	0.46	0.22	0.25	0.30	0.35	0.44	0.59
(19)	J035540.77+381549.9	0.01	0.51	0.18	0.20	0.24	0.28	0.34	0.44
(20)	J035916.33+400732.3	0.01	0.58	0.19	0.21	0.25	0.29	0.36	0.46
(21)	J041004.94+293102.0	0.04	0.76	0.37	0.43	0.50	0.60	0.75	1.00
(22)	J041116.70+221522.4	0.09	0.81	0.55	0.64	0.75	0.92	1.18	1.62
(23)	J050854.93+303039.0	0.15	0.64	0.62	0.73	0.88	1.11	1.46	2.08
(24)	J060253.72+003558.4	0.32	0.55	0.86	1.03	1.28	1.65	2.28	3.44
(25)	J060418.87+250218.8	0.05	0.74	0.40	0.46	0.54	0.65	0.82	1.10
(26)	J063023.56+210952.8	0.08	0.61	0.45	0.53	0.63	0.77	0.99	1.37
(27)	J072225.45+220525.8	0.03	0.42	0.25	0.29	0.34	0.41	0.52	0.71
(28)	J081035.34+230444.9	0.02	0.55	0.22	0.25	0.29	0.34	0.42	0.55
(29)	J090826.14+123648.2	0.07	0.18	0.22	0.26	0.32	0.41	0.55	0.82
(30)	J093507.99+270049.2	0.02	0.47	0.21	0.23	0.27	0.33	0.41	0.54
(31)	J093524.14+110836.2	0.03	0.92	0.39	0.45	0.52	0.62	0.77	1.01
(32)	J094811.23+552728.2	0.02	0.74	0.25	0.28	0.32	0.38	0.47	0.61
(33)	J104444.64+190229.6	0.04	0.72	0.37	0.42	0.49	0.59	0.74	0.99
(34)	J104531.95+582901.5	0.08	0.55	0.42	0.49	0.58	0.72	0.93	1.28
(35)	J161922.13+081914.3	0.01	0.62	0.21	0.23	0.27	0.32	0.39	0.50

a) and b) The serial number and designation of the targets, which are the same as Table 1. c) The minimum mass function. d) The estimated mass of the K/M-dwarf companions. e)-j) The estimated mass of the unseen objects with six uniform inclinations in sine, i.e., $\sin i = 1, 0.9, 0.8, 0.7, 0.6$ and 0.5 .

Table 3 Radial velocity measurements of of sources No. 5 and No. 7.

No.	obsdate	S/N _r	JD ₀	V _R (km s ⁻¹)
a)	b)	c)	d)	e)
No.5	2014 Jan. 22	59.44	6680.129167	105.1 ± 5.3
			6680.150694	-21.8 ± 5.4
			6680.172917	-133.1 ± 5.3
	2015 Mar. 22	71.48	7103.971528	82.1 ± 5.2
			7103.990972	-42.0 ± 5.3
			7104.011111	-142.9 ± 5.3
No.7	2014 Dec. 12	32.79	7004.281250	-57.1 ± 5.9
			7004.300694	-23.6 ± 6.5
			7004.320833	29.4 ± 6.3
	2015 Jan. 02	27.40	7025.177083	-158.2 ± 32.6
			7025.196528	-114.2 ± 7.7
			7025.215972	-74.2 ± 6.3
	2015 Mar. 07	16.98	7088.976389	-29.68 ± 11.8
	2015 Mar. 18	65.93	7099.978472	122.8 ± 5.2
			7099.997917	142.0 ± 5.3
			7100.017361	153.3 ± 5.4
	2016 Jan. 12	42.92	7400.180556	-95.4 ± 5.6
			7400.201389	-128.8 ± 5.6
			7400.220833	-144.2 ± 6.5
	2016 Nov. 10	97.44	7703.353472	-58.0 ± 5.1
			7703.372917	-97.0 ± 5.1
			7703.393056	-98.6 ± 12.6

a) the number of the source.

b) target observation date (Beijing time).

c) the signal-to-noise ratio in the r-band.

d) Julian Date (JD – 2, 450, 000).

e) radial velocity measured by the single epoch spectra.

5 Supplementary Material

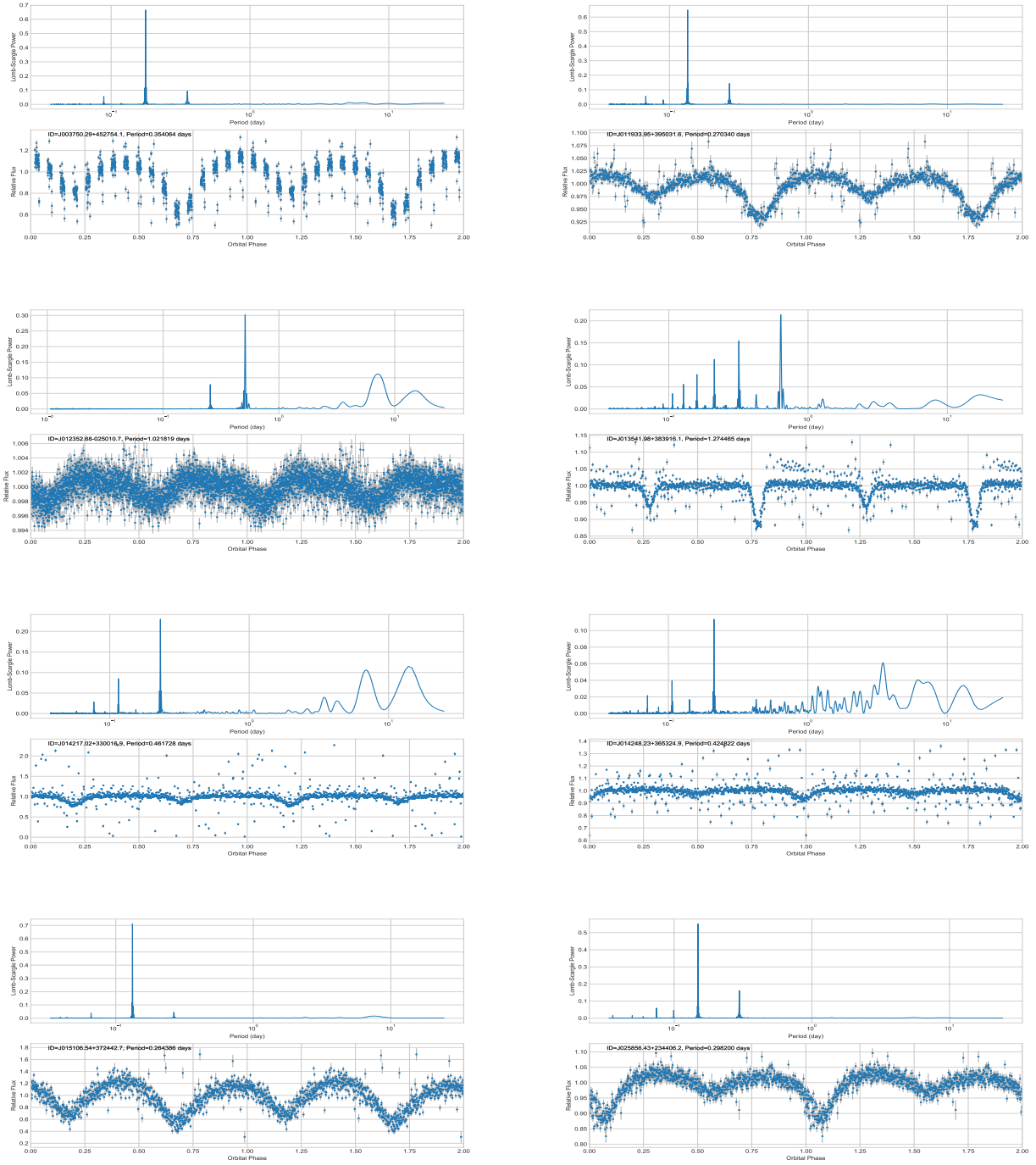


Figure S1 TESS light curves of the discarded eclipsing binaries.

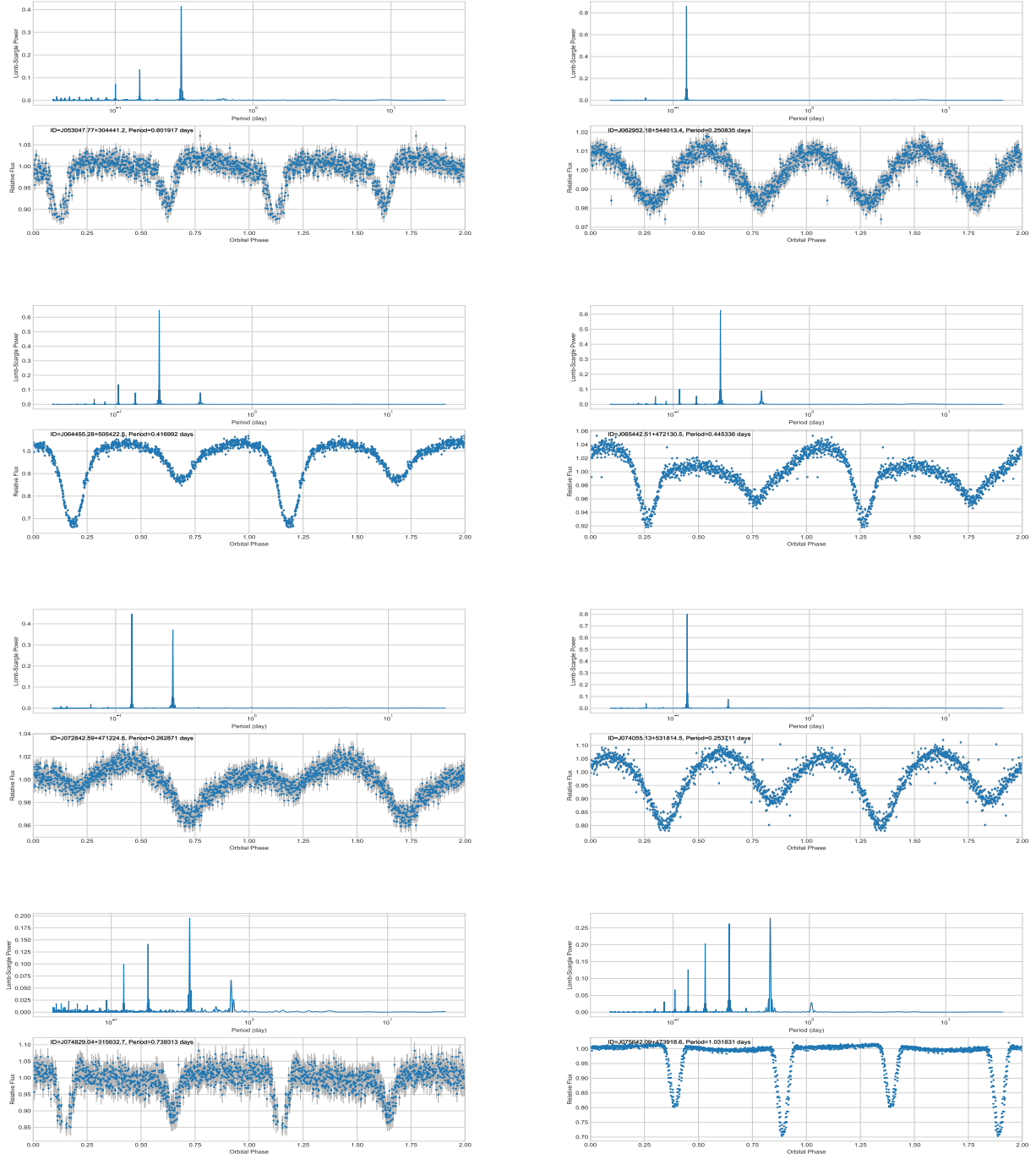


Figure S1 Continued.

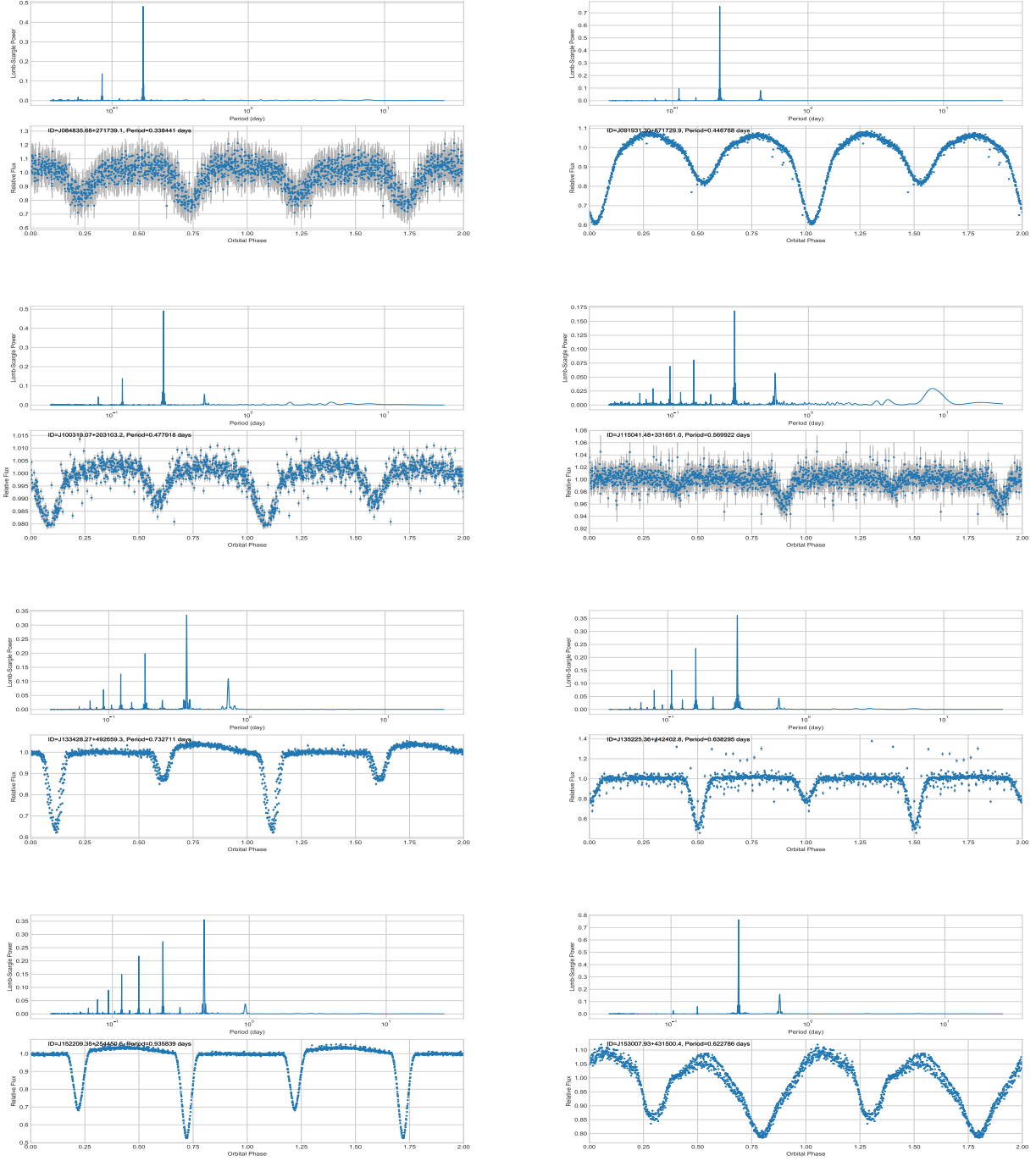


Figure S1 Continued.

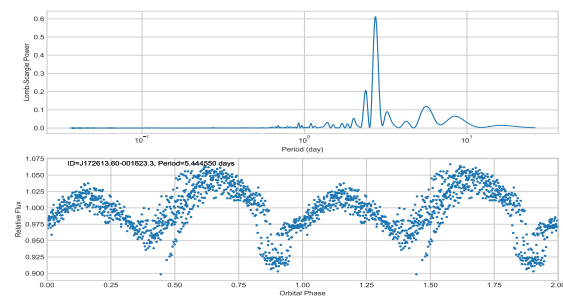


Figure S1 *Continued.*

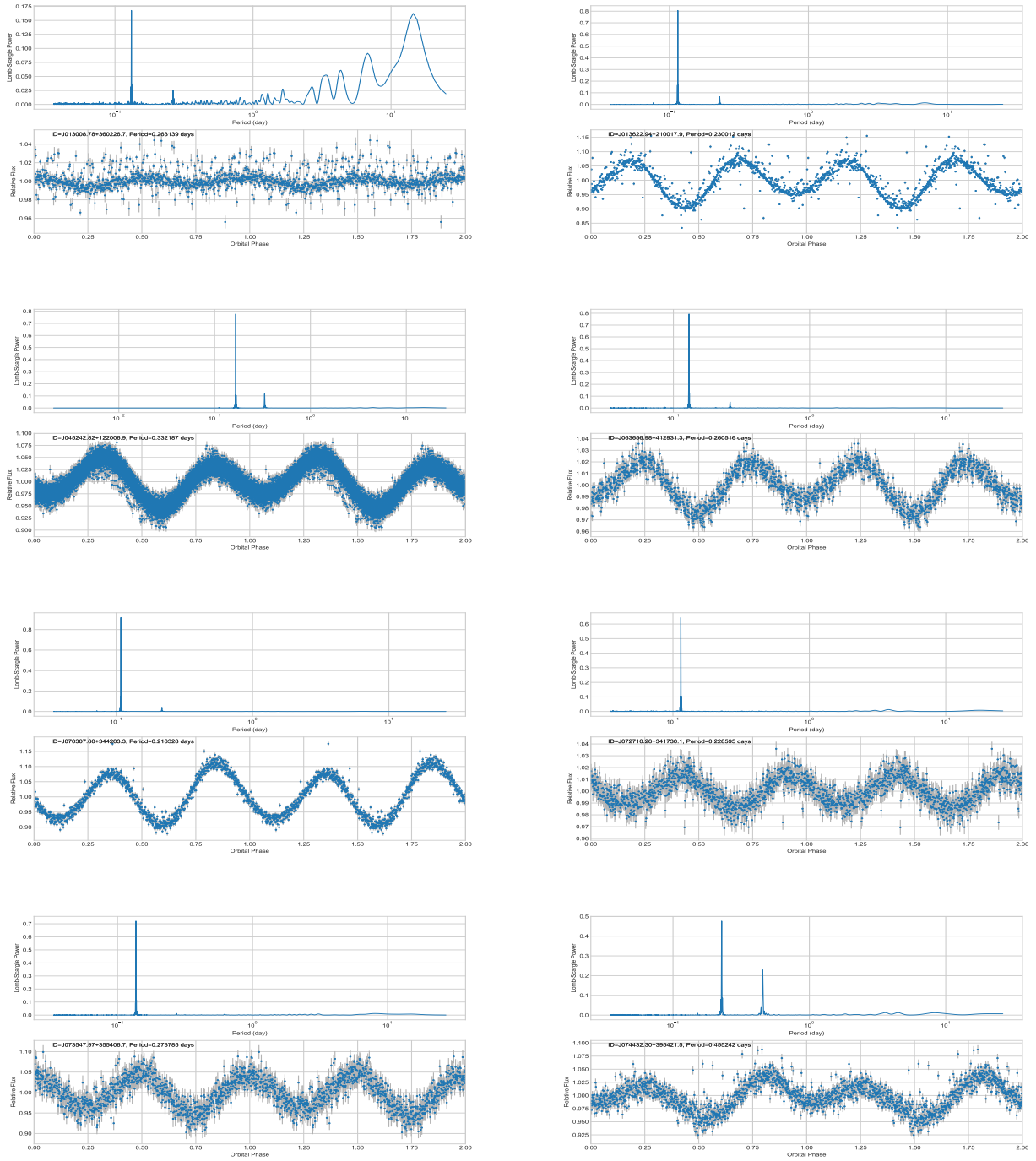


Figure S2 TESS light curves of ellipsoidal variables.

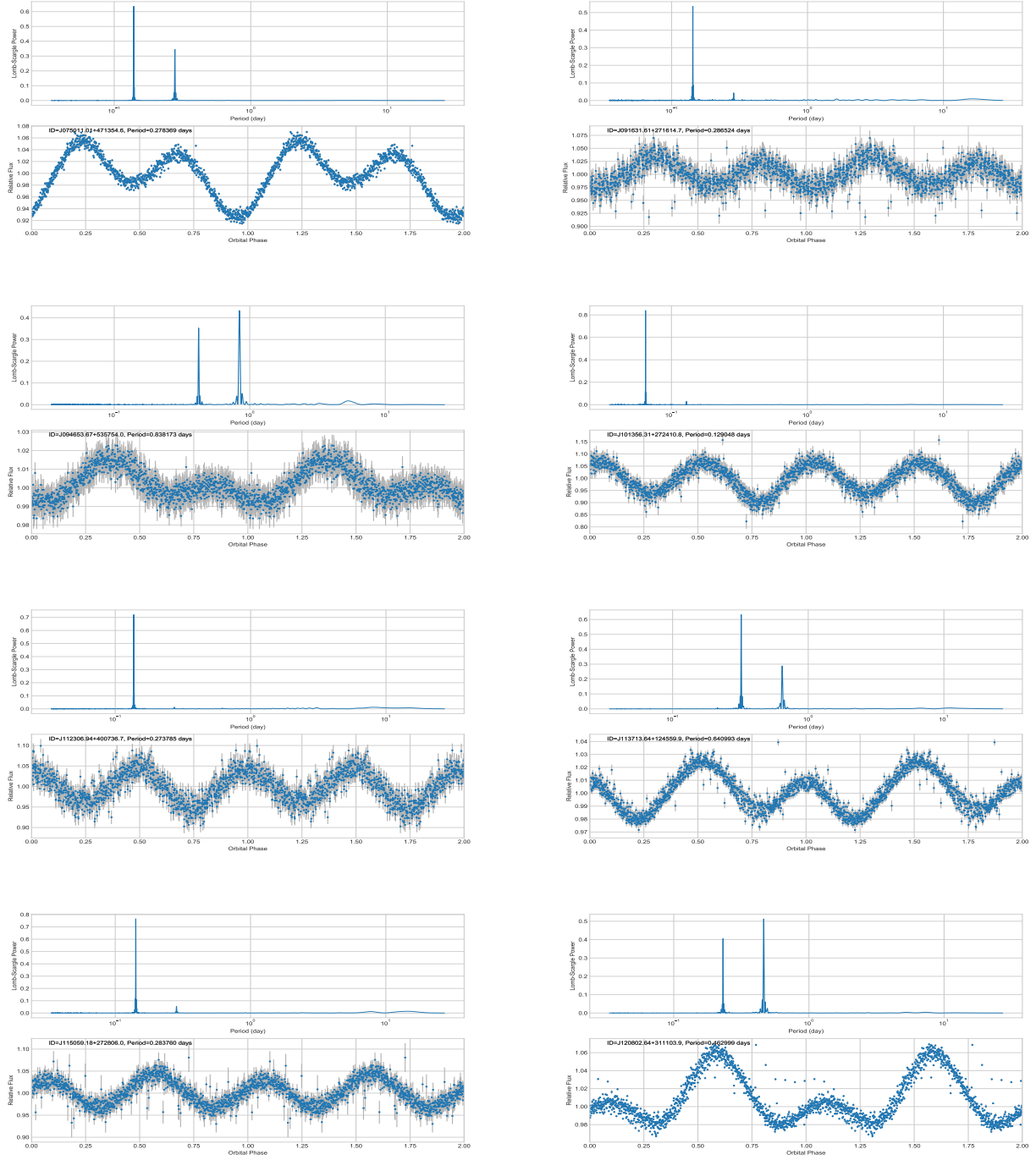


Figure S2 Continued.

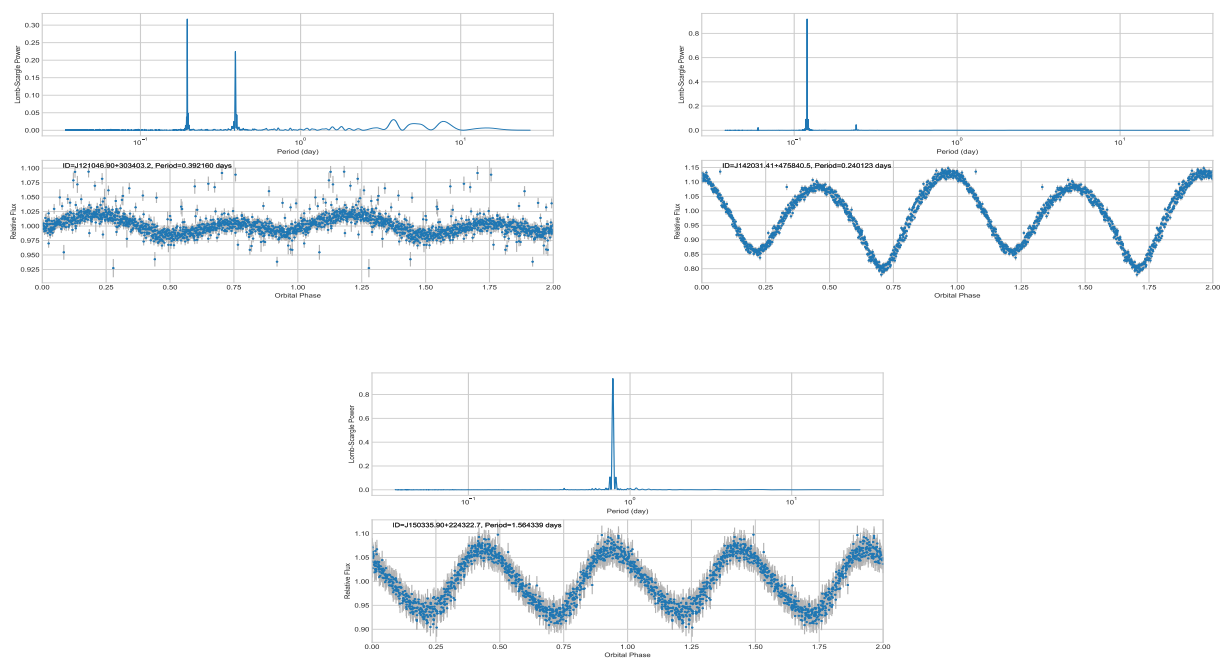


Figure S2 Continued.

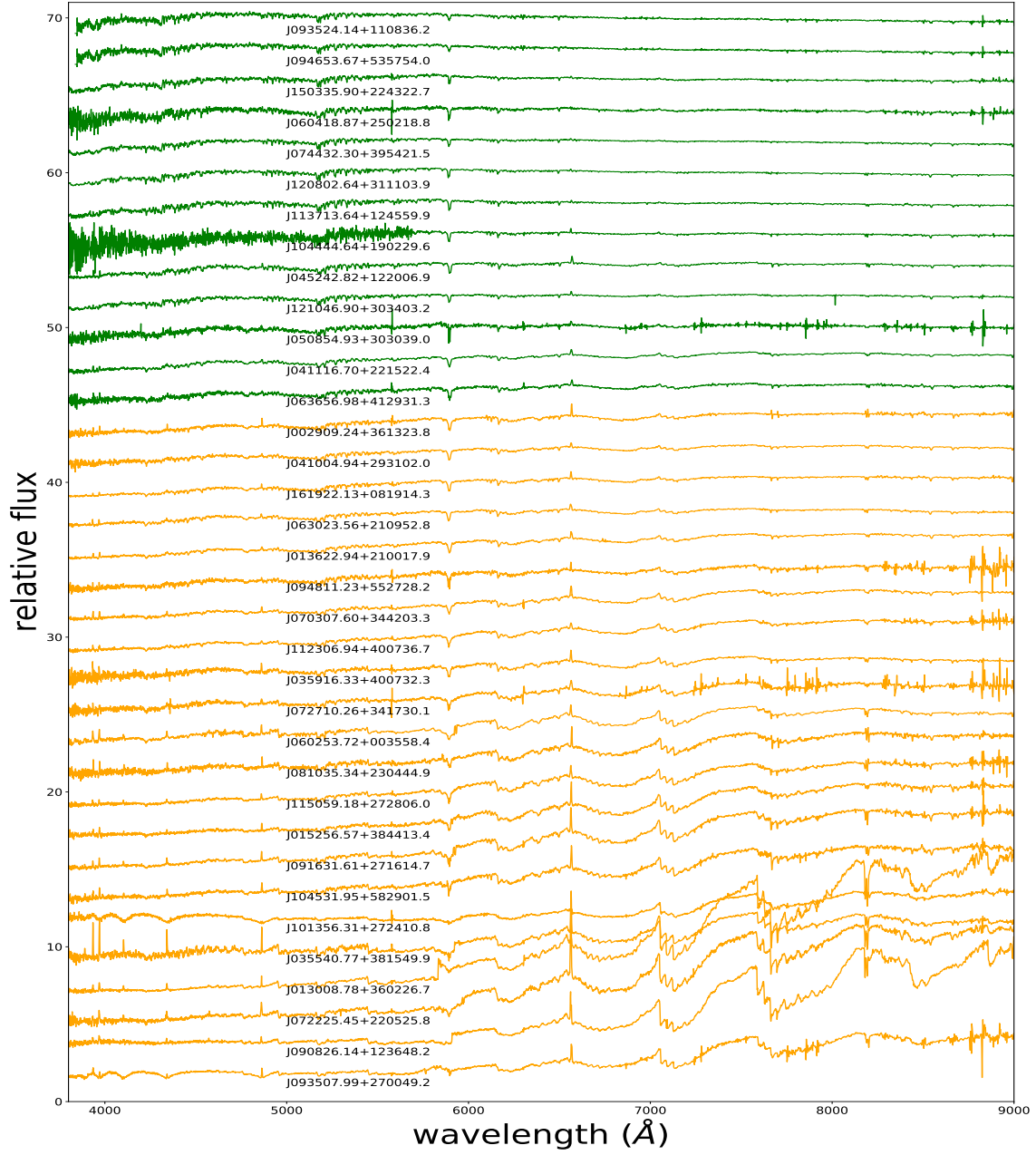


Figure S3 The combined spectra of the 35 sources provided by LAMOST. The olive spectra above and the orange spectra below represent the K-type and M-type of the PyHammer classification, respectively.

Table S1 Gaia astrometric quality flags for K/M-dwarfs in our sample.

Designation	ruwe	ϵ_i	BP/RP flux excess	Designation	ruwe	ϵ_i	BP/RP flux excess
[1]	[2]	[3]	[4]	[5]	[6]	[7]	[8]
J001057.66+470307.2	0.954	0	1.3	J074432.27+395421.8	1.045	0.031	1.25
J002909.24+361323.8	1.046	0.112	1.338	J074829.03+315632.7	1.014	0	1.286
J003750.29+452754.1	0.947	0	1.303	J075011.01+471354.6	1.007	0	1.275
J011933.95+395031.7	1.066	0.089	1.246	J075642.26+473917.9	0.926	0	1.252
J012352.68-025010.7	1.407	0.223	1.266	J081035.34+230444.9	1.033	0.052	1.394
J013008.78+360226.7	1.133	0.13	1.505	J084835.68+271739.1	0.978	0	1.205
J013541.98+383916.1	1.484	0.276	1.297	J090826.14+123648.2	1.144	0.121	1.529
J013622.94+210017.9	1	0	1.339	J091631.62+271614.8	1.013	0	1.416
J014217.02+330016.9	8.18	2.469	1.532	J091931.31+571730.2	1.419	0.119	1.227
J014248.23+365324.9	1.018	0.072	1.277	J093507.99+270049.2	1.08	0.021	1.433
J015106.54+372442.7	1.032	0.059	1.37	J093524.14+110836.2	1.151	0.171	1.251
J015256.57+384413.4	1.006	0	1.399	J094653.65+535754.5	1.006	0	1.294
J025856.43+234406.2	1.062	0.089	1.281	J094811.23+552728.2	1.04	0	1.402
J033655.85+192321.5	1.023	0	1.268	J100319.08+203103.2	0.989	0	1.253
J034210.62+384219.9	0.994	0	1.277	J101356.31+272410.8	1.072	0.159	1.416
J035540.77+381549.9	1.058	0.101	1.463	J104444.64+190229.6	1.053	0.076	1.28
J035829.70+232454.3	0.954	0	1.258	J104531.95+582901.5	1.007	0	1.389
J035916.33+400732.3	0.959	0	1.374	J112306.94+400736.7	1.008	0	1.365
J040441.99+022425.1	0.989	0	1.402	J113326.70+313108.1	1.03	0.028	1.29
J041004.94+293102.0	1.498	0.383	1.385	J113713.64+124559.9	1.023	0	1.246
J041116.70+221522.4	1.012	0	1.391	J114114.74-050825.5	1.067	0.099	1.31
J045242.82+122006.9	1.092	0.026	1.324	J115041.48+331651.0	1.039	0.769	1.423
J050854.93+303039.0	1.018	0.037	1.344	J115059.18+272805.8	1.086	0.086	1.385
J053047.77+304441.2	1.029	0	1.31	J120803.04+311103.9	1.025	0.13	1.253
J053757.36+220843.0	1.01	0.057	1.276	J121046.90+303403.4	1.29	0.175	1.292
J060253.72+003558.4	1.206	0.092	1.424	J123151.59+252230.8	0.908	0	1.257
J060418.87+250218.8	0.979	0	1.306	J123529.01+255425.4	0.946	0	1.273
J062952.18+544013.4	1.17	0.147	1.244	J133428.27+492659.3	1.095	0.038	1.28
J063023.56+210952.8	0.979	0	1.346	J133751.25+360653.0	4.242	0.479	1.288
J063656.98+412931.3	1.006	0	1.347	J135225.36+442403.1	1.02	0	1.278
J064455.26+505423.6	1.342	0.195	1.317	J140408.29+035337.0	1.044	0.067	1.253
J065442.51+472130.5	3.927	0.515	1.239	J142031.41+475840.5	1.991	0.327	1.263
J070307.60+344203.3	1.057	0.063	1.344	J150335.90+224322.7	1.021	0.038	1.26
J071349.17+154644.4	0.982	0	1.238	J150916.03+360200.1	0.996	0.059	1.224
J071934.24+321719.4	0.972	0	1.273	J152209.35+254450.5	1.34	0.103	1.283
J072225.45+220525.8	0.918	0	1.449	J152843.82+205140.2	1.04	0.047	1.272
J072652.92+272232.1	8.265	1.512	1.48	J153007.93+431500.4	1.084	0.076	1.201
J072710.26+341730.1	0.978	0	1.362	J153854.15+361453.3	0.998	0.028	1.286
J072842.59+471224.6	0.934	0	1.325	J161922.13+081914.3	1.049	0	1.32
J073547.97+355406.7	1.034	0.054	1.248	J172613.60-001623.3	0.898	0	1.281
J074055.15+531814.4	1.054	0.048	1.302				

[1] and [5]: target designation.

[2] and [6]: the renormalised unit weight error.

[3] and [7]: excess noise of the source: astrometric_excess_noise.

[4] and [8]: BP/RP flux excess factor: phot_bp_rp_excess_factor.